Title
BEAM ANALYZING SYSTEM FOR A VARIABLE ENERGY CYCLOTRON

Authors
Hintz, R.E.
Selph, F.B.
Flood, W.S.
et al.

Publication Date
1968-08-01

UCRL-18383

BEAM ANALYZING SYSTEM FOR A VARIABLE ENERGY CYCLOTRON

R. E. Hintz, F. B. Selph, W. S. Flood,
B. G. Harvey, F. G. Resmini
and E. A. McClatchie

August 1968

LAWRENCE RADIATION LABORATORY
UNIVERSITY of CALIFORNIA BERKELEY

UCRL-18383

DISCLAIMER

To be submitted to:
Nuclear Instruments and Methods

UCRL-18383
Preprint

UNIVERSITY OF CALIFORNIA

Lawrence Radiation Laboratory
Berkeley, California 94720

AEC Contract No. W-7405-eng-48

BEAM ANALYZING SYSTEM FOR A VARIABLE ENERGY CYCLOTRON

R. E. Hintz, F. B. Selph, W. S. Flood, B. G. Harvey,
F. G. Resmini and E. A. McClatchie

August 1968

BEAM ANALYZING SYSTEM FOR A VARIABLE ENERGY CYCLOTRON*

R. E. Hintz, F. B. Selph, W. S. Flood, B. G. Harvey,
F. G. Resmini† and E. A. McClatchie

Lawrence Radiation Laboratory
University of California
Berkeley, California 94720

August 1968

ABSTRACT

A new beam analysis system has been installed at the Berkeley 88" cyclotron. The system consists of two 110° flat field, edge focusing bending magnets. The first magnet is used to energy analyse the cyclotron beam, and the second or "clean up" magnet is used to remove slit scattered particles produced by the analysing magnet. The system has achieved its design performance of 0.02% energy resolution, with a long term stability of two parts in 10^5. Up to 0.6 μ A of a beam with a radial emittance of 4.5 mm mrad has been obtained with the above energy resolution.

This paper describes the design, construction, installation shimming and testing of the magnets, as well as the construction of the regulated power supply.

---

*Work performed under the auspices of the U. S. Atomic Energy Commission.

†Permanent address: University of Milan, Physics Institute.

1. Introduction

The Berkeley 88-inch cyclotron produces very intense beams of protons (10-55 MeV), deuterons (10-65 MeV), ^{3}He (20-150 MeV) and ^{4}He (23-130 MeV) with small emittance and an energy resolution of 0.2-0.4% (full width at half maximum). For several years the energy resolution obtained in nuclear reaction and scattering experiments has been limited by the resolution of the best analyzed beam (which has 0.08% FWHM) rather than by the counting equipment.

A new beam-analyzing system has been built to permit experiments to be done with better energy resolution. Since it seemed probable that silicon and germanium particle counters would eventually be capable of better than 0.05% resolution, a value of 0.02% was chosen as the desired beam resolution. (It has indeed been found that both Si(Li) and Ge(Li) counters can give resolutions of 0.04% including electronic noise and the energy spread of the beam itself.) Of equal importance was the removal of "tails" (due to slit scattered particles) in the primary beam.

Two identical uniform-field magnets were constructed. In the normal mode of operation the first magnet acts as the energy analyzer while the second magnet is used to remove beam tails. Referring to Fig. 1, the beam is transported from the cyclotron and brought to a horizontal focus at the entrance slit. This slit -- normally set at a gap width of 1/2 mm -- defines a source for the first (analysing) magnet. An energy-dispersed image of the slit is formed at the analyzing slit, which is at the radial focus of magnet one. The analyzing slit, again normally set at 1/2 mm gap, is used to energy-analyze the beam and to provide a source for magnet two. At the radial focus of the second magnet an image of the analyzing slit is formed. The slit scattered particles have lower energy and thus a third slit (the clean-up slit) can be used to remove

these particles. The clean-up slit is normally set to 2-5 mm gap to avoid further scattering of the beam. A photograph of the second magnet in its installed position is shown in Fig. 1a.

Since the magnets are disposed in such a way that their dispersions add, closure of the clean-up slit to 0.5 mm should in principle give a beam with twice as good an energy resolution as that obtained at the analyzing slit; i.e, the energy resolution (FWHM) should be better than 0.01%. This has not been checked.

The remaining features of the beam transport system (e.g., the 20° bend prior to entry into the analyzing magnet) were largely dictated by the necessity of conforming to an existing floor plan.

2. Selection of Parameters, Resolution, Aberrations

A flat field, edge focusing design with equal entrance and exit angles was chosen for the analyzing magnet because of the mechanical simplicity of such a design. Entrance and exit edges were made straight, with inside corners beveled (Fig. 2). Field clamps were used to limit the fringing fields, to make the fringing fields as uniform as possible in a direction parallel to the pole pieces, and to shield the magnet ends from outside pieces of iron.

Methods of calculating the focusing properties of uniform field magnets have been discussed by several authors. See the review article of Enge[1]). For this magnet, the necessary parameters are α, the turn angle; β, the edge angle; ρ, the magnet radius; the radial source and image distances ℓ_{sx}, ℓ_{fx} and the radial magnification m_x, (Fig. 3). Corresponding axial quantities are denoted with a subscript y. We find that these quantities can be conveniently expressed by the equations:

$$\ell_{sx} = \rho \frac{m_x(\cos\alpha + \sin\alpha \tan\beta) - 1}{m_x[\sin\alpha\,(1 - \tan^2\beta) - 2\cos\alpha \tan\beta]} \tag{1}$$

$$\ell_{fx} = \rho \frac{\cos\alpha + \sin\alpha \tan\beta - m_x}{\sin\alpha\,(1 - \tan^2\beta) - 2\cos\alpha \tan\beta} \tag{2}$$

$$\ell_{sy} = \rho \frac{m_y(1 - \alpha \tan\beta) - 1}{m_y(2 \tan\beta - \alpha \tan^2\beta)} \tag{3}$$

$$\ell_{fy} = \rho \frac{1 - \alpha \tan\beta - m_y}{2 \tan\beta - \alpha \tan^2\beta} \tag{4}$$

The first order resolution P_1 of the system when used with an analyzing slit of width x_f we define as the value of $\Delta p/p$ which will just be transmitted by the slit.* In terms of magnet parameters α, β, ρ we find

$$P_1 = x_f \left[\rho(1 - m_x)\left(1 + \frac{\tan\beta\,(1 + \tan\beta \sin\alpha + \cos\alpha)}{\sin\alpha - 2 \tan\beta \cos\alpha - \tan^2\beta \sin\alpha}\right)\right]^{-1} \tag{5}$$

The resolution is improved by making x_f small and ρ large. Experience with analyzing slits suggested $x_f = 0.5$ mm as the smallest value which could safely be used for design. A value for the maximum magnetic field well below 10 kG was desired in order to avoid saturation effects. A value of $\rho = 2.032$ m (80") was chosen which gives a field of 8.15 kG for 130 MeV α particles. The desire to achieve a compact layout favored a large value for α. Adequate vertical focusing determines the choice of β. A design in which the radial and vertical sources were separated was wanted in order to lessen the power per square cm. deposited on the source slit. The values chosen were $\alpha = 110°$,

*Assuming uniform illumination on a source slit of width $x_s \leq x_f/|m_x|$.

$\beta = 38°$. It was decided to operate, initially at least, with $m_x = -1$ and with a symmetrical two-magnet system. In this case, eqs. 1-5 give

$$\ell_{sx} = \ell_{fx} = \ell_{fy} = 3.1413 \text{ m} \tag{6}$$

$$\ell_{sy} = 2.111 \text{ m} \tag{7}$$

$$P_1 = 5.57 \times 10^{-5}$$

In operation, the exact vertical focal distance is not of much importance as one simply wants to keep a reasonable vertical beam size through the magnet. Figure 4 shows typical beam envelopes in the magnet. The maximum radial and vertical amplitudes of beam in the magnet can be controlled with collimators placed upstream (the x- and y-collimators, Fig. 1).

Aberrations were studied with the aid of a digital computer program which integrates the equations of motion. The magnetic field was supplied by dividing the magnet into regions and in each region using a suitable analytic approximation to the field. In the center region magnet curvature was neglected and a two dimensional representation used. Taking r as a coordinate measured from the magnet centerline in a radial direction, and z in an axial direction, we can express magnetic fields as power series in r, z:

$$B_r = -A_o - A_1 r + B_1 z - A_2 r^2 + A_2 z^2 + 2B_2 rz \tag{9a}$$

$$B_z = B_o + B_1 r + A_1 z + B_2 r^2 - B_2 z^2 + 2A_2 rz \tag{9b}$$

These expressions satisfy Maxwell's equations in two dimensions. Neglect of the curvature introduces errors in the first derivative that are of the order of r/z in the present case amounting to at most 3%, which is not significant.

At the ends of the magnet, each fringe field is divided into two regions, in each of which expressions such as (9) are used to represent the field. Continuity can be satisfied only on the magnet center line, so that sizable field errors occur for particles off the axis by more than about 1 cm. However, since the fringe field regions are relatively short, the resulting orbit errors are small.

The image of a point source, traced through a uniform field ($B_r = 0$, $B_z = B_o$) is shown in Fig. 5. Results are plotted in the x, x' plane. Particles which leave the source on the line $x = 0$ lie in the image plane on an approximately parabolic curve. As this median plane aberration is proportional to x'^2 it can be eliminated by causing some part of the magnetic field to vary with r^2. This is often done by curving the entrance and exit edges[1]). In the present case it was decided that shimming the field was a more practical method, because the shims could be cut after field measurements had been made. The shims could then correct for the expected field sag, as well as introduce the required r^2 shaping.

Putting all coefficients zero except for B_o, B_2 in eqs. (9) gives

$$B_r = 2B_2 rz \tag{10a}$$

$$B_z = B_o + B_2 (r^2 - z^2) \tag{10b}$$

In the median plane ($z = 0$) this field has the desired variation with r^2. The median plane aberration can be reduced to $\Delta x \leq 5.5 \times 10^{-3}$ for $|x'| \leq 12$ mrad with the values

$$B_2/B_o = -4.41 \times 10^{-6} \text{ cm}^{-2} \quad \text{for} \quad r > 0$$

$$B_2/B_o = -4.66 \times 10^{-6} \text{ cm}^{-2} \quad \text{for} \quad r < 0.$$

The corrected curve is shown as 1 in Fig. 6. The coefficients are not affected by the manner in which the fringe field falls off, so long as it is uniform in a direction parallel to the pole edges. Particles off the median plane experience a different bending field (proportional to z^2). This has principally the effect of shifting the focal point in the image plane. For a beam of 2 cm height, the shifts are $\Delta x \sim -0.2$ mm (curves 2 and 3, Fig. 6).

An estimate of the resolution which can be expected from the system can be made by plotting traces in x, x' image space of the particles with worst aberrations (Fig. 7). The figures corresponding to p and p + Δp which lie outside, but which touch the slit at some point inside $|x'_{max}|$ give the resolution, which is just $\Delta p/p$. As the only significant aberration remaining is the z^2 one, we can thus estimate that the first order resolution calculated above will be increased by the factor $(1 + \frac{\Delta x}{x_f}) = 1.4$ for a beam of 2 cm vertical height. As, with this increase, the theoretical resolution is still within the hoped for value of 1.0×10^{-4} no attempt was made to correct for the z^2 aberration.

3. Magnet Design

A number of precision analysis systems for cyclotrons have utilized gradient field magnets[2,3]. The purpose of the gradient field is to produce vertical focusing. We have chosen a uniform field "picture frame" design with edge focusing because of several advantages which this affords compared with the gradient design. A uniform field can be produced to a higher degree of precision and can be maintained over a wider range of field intensity. This insensitivity of field shape to field intensity is due primarily to the

elimination of pole tips. It was felt that magnetic field measurements, and shimming to produce the required field precision, would be much easier with uniform field magnets. Finally, the magnet weight of the present design is 5 tons, while the weight of a comparable gradient magnet is 25-50 tons. The cost was correspondingly low -- about $25,000 per magnet compared with an estimated $80,000 for a gradient magnet of similar performance.

The maximum field in the iron has been limited to 12 kG so that the change in permeability in the iron is minimized for a wide range of field intensity. The iron is a commercial grade of low carbon AISI C1010 steel rolled plate that was annealed at 1600° F for three hours.

The pole plates were machined flat to better than 0.001 inch within 20 inches. The spacers for both magnets were uniform in thickness to 0.001 inch. A cross section of the iron, coil and vacuum tank is shown in Fig. 8.

The entrance and exit pole corners were chamfered to minimize saturation effects (Fig. 2). The chamfering, as well as the location of the field clamps, were done in such a way as to minimize the change in effective field length with magnet excitation. For this work a field mapping computer program TRIM[4]) was used, which takes into account the finite permeability of the iron. This was only partly successful, as measurements show that the effective field boundary moves 0.8 cm as the field is raised from 2 to 8 kG.

Magnets which have the coil space restricted to the gap dimension require high current density. This is most easily obtained by using high currents in water-cooled conductors. The present magnets are operated in series to avoid the cost of building two high current precision regulators and to simplify operation. The magnet coils consist of 36 turns of 0.5 inch square copper

conductor with a 0.25 inch diameter hole. The power required per magnet at 1000 A is 50 kW. The corresponding magnetic field is 7,840 gauss.

The vacuum tanks were made from 4 1/2" (outside diameter) aluminum alloy tubing with a 0.120" wall thickness. After bending to 110° and annealing, the tubes were placed in position and flattened by carefully bolting down the upper steel plate of each magnet. A small recess was made near one end of each pipe to permit insertion of an NMR probe, far enough beyond the first shim to be in a region of uniform field.

4. Field Regulation

An existing 130 kW silicon controlled rectifier power supply was provided with a series transistor pass element designed to provide a long-term field stability of 1 part of 10^5. The pass element is a parallel array of three modular water-cooled heat sinks with 36 transistors situated on each. The module is a three stage Darlington emitter follower: a single transistor input stage drives an intermediate stage of five in parallel, which drives a 30 parallel-transistor output stage. All transistors are Westinghouse type 163-035. We rate a single module at 500 amperes or 6 kW. The d.c. current gain of the module is not less than 10^4 at rated current.

The two magnets are operated in series across the power supply; individual control is provided by shunt transistor trimmers permitting up to 2.2 A to be diverted around each magnet. This amount of individual control provides ample compensation for minor differences between the two magnets as well as for alignment errors.

The regulation scheme is shown in Fig. 9: the parameters are listed in Table 1. dB/dt coils (32 turns of No. 22 wire) were provided in each magnet. Current regulation is provided by the water-cooled manganin shunt as well as by the

dB/dt coils. Although provision was made for NMR regulation, it has been found that the long-term stability of the current regulator is greater than that of any available NMR oscillator. Hence the NMR system is used to measure - but not to control - the magnetic field.

Residual fields are controlled before each experiment by slowly raising the magnet current from zero to maximum, then slowly lowering it to zero and finally returning slowly to the desired value. This routine was also followed during the magnetic field measurements.

During the course of several long experiments, the field stability has been excellent. The largest field variation that has been observed during periods of 24 hours is 2 parts in 10^5.

5. Field Measurements

Magnetic field measurements were made only in the median plane of the magnets, using coils and a precision integrator. The central region (24 inches from each pole edge) was studied with a point-measuring coil that could be moved azimuthally at a given radius, or along a radius at a given azimuth. The two ends of each magnet were studied with long coils that extended from 16 inches outside the magnet to 24 inches inside. The radial field variation was studied by moving the long coils parallel to the pole edge. All measurements were made at three field values -- approximately 2, 5 and 8 kG.

Figure 10 shows azimuthal scans with the point-measuring coil at the beam exit end of a magnet at three different radii. Planimeter integration between -10" and +10" showed that the effective position of the field boundary moved from -0.43 ± 0.25 cm at 2 kG to $+0.36 \pm 0.25$ cm at 8 kG.

Figure 11 shows azimuthal scans of the central part of the field at several radii. By planimeter integration of such curves at each field level

to within 24 inches from each pole edge, the radial variation of the azimuthally averaged field was obtained, with the results shown in Fig. 12. The radial variation at all three field levels could be fitted very closely by the parabola

$$\frac{\bar{B} - \bar{B}_o}{\bar{B}_o} = \frac{\bar{B}_2}{\bar{B}_o} (r + D)^2$$

where $\bar{B}$ is the average field at a radius r from the central radius, $\bar{B}_o$ is the average field at r = 0 and D is the displacement of the vertex of the parabola from r = 0. The second order coefficients $\bar{B}_2/\bar{B}_o$ and the displacements D have the values shown in Table 2. By suitable shimming (v. infra) the coefficients were modified to the desired values.

Figure 13 shows an example of the radial variation of the field at the end of a magnet, measured with the long coil. The field clearly does not vary with radius in a parabolic manner. The radial variation was fit to an equation containing a linear term which could arise if the coil motion was not perfectly parallel to the pole edge:

$$\frac{\bar{B} - \bar{B}_o}{\bar{B}_o} = \frac{\bar{B}_1}{\bar{B}_o} (r + D) + \frac{\bar{B}_2}{\bar{B}_o} (r + D)^2$$

The points in Fig. 13 show the fit of this equation for $\bar{B}_1/\bar{B}_o = -17.2 \times 10^{-5}$ in^{-1}, $\bar{B}_2/\bar{B}_o = -26.0 \times 10^{-5}$ in^{-2} and D = -0.72 in. Shims were designed for each end region to correct only $\bar{B}_2/\bar{B}_o$ to the desired value.

The values of $\bar{B}_2/\bar{B}_o$ and D (averaged for the three field values) for the two magnets are shown in Table 2. Observe that the field shapes at the ends of the magnets vary widely, and the parabolic variation is in the opposite sense to that of the central region.

6. Shim Design

Each azimuthal region of the field was corrected to the desired value of $\bar{B}_2/\bar{B}_o$ by means of properly shaped pairs of shims cut from 0.015"-thick iron stock and attached one above the other to the upper and lower pole surfaces with Loktite 404 cement. After completion of the field measurements it was of course necessary to remove the upper pole of each magnet to permit installation of the shims and the vacuum tank. It was established that the field shape remained undisturbed provided that the bolts were always tightened to the same torque. One pair of shims was used for each end-region and two pairs for each center region.

The result of shimming in this way is to obtain a field in each region for which the field integral along an azimuthal path at constant radius varies with radius in the desired manner. Particles, however, do not follow such paths, and it would be somewhat better to shim the field point by point by re-machining the pole surfaces. If necessary, a correction can be made to allow for shimming at a small number of discrete azimuths rather than continuously.

Consider a field region of length $\ell(r)$ measured along a path of radius $(R_o + r)$. Let the region be bounded at one end by a surface making an angle β to a radius and at the other end by a radial surface, as shown in Fig. 14. The angle subtended by the field region is α.

$$\ell(r) = R_o \alpha + r(\alpha - \tan \beta) \tag{11a}$$

Let the average unshimmed field be

$$\bar{B}_u(r) = B_o^{(1)} + B_2^{(1)} (r + D)^2 \tag{11b}$$

where D is the radial displacement of the field minimum from R_o.

Let the desired field be

$$\bar{B}_s(r) = B_o^{(2)} + FB_2^{(2)} r^2 \tag{11c}$$

where the factor F corrects for the difference between a discrete number of shim pairs and a continuous field correction. In the present geometry such effects are negligible and we can set F equal to 1.

For a shim pair of combined thickness t in a pole gap h, the field within the shims is greater than the field just outside a shim by the ratio h/(h-t). With N shim pairs, each of width S(r)

$$\begin{aligned} \bar{B}_s(r) &= \bar{B}_u(r) \left[1 + \frac{N\, t\, S\,(r)}{(h - t)\ell(r)}\right] \\ &= \left[B_o^{(1)} + B_2^{(1)} (r + D)^2\right]\left[1 + \frac{N\, t\, S\,(r)}{(h - t)\ell(r)}\right] \end{aligned} \tag{12}$$

$$\therefore B_o^{(2)} + B_2^{(2)} r^2 = \left[B_o^{(1)} + B_2^{(1)} (r + D)^2\right]\left[1 + \frac{N\, t\, S\,(r)}{(h - t)\ell(r)}\right] \tag{13}$$

At r = 0

$$B_o^{(2)} = \left[B_o^{(1)} + B_2^{(1)} D^2\right]\left[1 + \frac{N\, t\, S\,(0)}{(h - t)\ell(0)}\right]$$

Substituting for $B_o^{(2)}$ into eq. (13); and solving for S(r), we find

$$S(r) = \frac{(h - t)\ell(r)}{Nt}\left(\frac{B_s(r)}{B_u(r)} - 1\right) \tag{14}$$

where $B_u(r)$, $B_s(r)$ and $\ell(r)$ are given by eqs. (11a,b,c). The central width of a shim S(0) is quite arbitrary: it was chosen so that the shim width remained greater than 1" at any value of r.

A template for each pair of shims was cut from 1/8" brass sheet and adjusted with a filing machine to the correct contour within an accuracy of about 0.002". The 0.015" shim stock was cut and adjusted by hand to fit the template.

The exact position of a shim within its field region is unimportant. The end-region shims were placed on the flat part of the poles as close as possible to the pole edges. The two pairs of center-region shims were placed symmetrically about the center of the magnet at an azimuthal angle of about 41° from the pole edges.

The whole system was successfully operated eight working days after completion of the last field measurements.

7. Energy Resolution Measurements

7.1 MAGNET SWEEPING

The energy resolution obtained from the first magnet can be rapidly measured with the second magnet. The clean-up slit is closed to 0.25 - 0.5 mm and the field of the second magnet is adjusted to give maximum beam intensity in the Faraday cup. The beam is then swept across the clean-up slit by raising and lowering the field to the values that give beam intensities of half the maximum value. If ΔB is the range of the field variation, one has, in first approximation

$$\left(\frac{\Delta E}{E}\right)_{FWHM} = \frac{2\Delta B}{B} = \frac{2\Delta I}{I}$$

Typically, a value of $\Delta E/E$ in the range 0.02 - 0.025% is obtained.

After correction for finite slit widths the values of $\Delta E/E$ for a wide variety of beam particles and energies fall in the range 0.015 - 0.020%. (The method of correction is described in the Appendix.)

7.2. ^{12}C PROTON RESONANCE

A further test was made by measuring the well-known[5]) T = 3/2 resonance in a ^{12}C target at a proton energy of 14.233 MeV. Protons scattered at 165° (lab) from a 15 $\mu g/cm^2$ natural carbon target were detected in two Si(Li) counters, with the results shown in Fig. 15. The sharp drop between the maximum and minimum cross sections occurs within a 2 keV energy change. The beam energy resolution (FWHM) must therefore be of the order of 2 keV, or 0.014%. This value, as well as the values obtained in method (a), is very close to the calculated value for a perfectly corrected field (0.011 - 0.015%, depending on the vertical extent of the beam in the magnets). It must be emphasized that this result was obtained with only the first magnet acting as an analyzer. The clean-up slit of the second magnet was wide open.

At this resolution level, the beam intensity at the target position is typically a few hundred nanoamps with a radial emittance of 4.5 mm - mrad. By opening the source and image slits of the first magnet to 1 mm (twice their normal width), the beam intensity increases fourfold with only a twofold loss of resolution.

By opening all slits and making a radial focus at a point about half way between the entrance slit and the analyzing magnet, a dispersionless solution is obtained. Approximately 50% of the total cyclotron beam can be focused on to the target.† This mode of operation will be valuable because it allows experiments with beams of polarized protons in the 36" scattering chamber.

---

†We are indebted to Drs. J. Ernst, R. de Swiniarski and A. D. Bacher for investigating the dispersionless solution.

ACKNOWLEDGMENTS

We wish to acknowledge the important contributions made by H. Johnson, Milton Hom, Lewis Chase, R. F. Burton, A. Hartwig, J. R. Meneghetti, and the staffs of the cyclotron Accelerator Technician and Electrical shops. P. G. Watson kindly provided the equipment for field measurements and instructed us in its use.

REFERENCES

1) H. A. Enge, in Focusing of Charged Particles, A. Septier, (ed.), pp. 203-264, vol. II, Academic Press (1967)

2) J. Bardwick, J. M. Lambert, and W. C. Parkinson, Nucl. Instr. and Methods 18, 19 (1962) 105

3) The Oak Ridge Isochronous Cyclotron, Annual Progress Report for period ending Dec. 31, 1964. Report ORNL 3800

4) A. M. Winslow, Proc. Int. Symposium on Magnet Technology, Stanford, 1965, p. 170

5) J. B. Marion, Revs. of Modern Physics 38 (1966) 660

APPENDIX

Correction of measured $\Delta E/E$ values for finite slit widths

In order to get a better estimate of the energy resolution given by the first magnet from the measurements made with the second magnet a more precise analysis has been carried out.

We have calculated the beam current distribution at the image slit under the following assumptions:

1) The aberrations in the second magnet are neglible.

2) Consequently the dispersive power of the magnet is assumed to be the calculated one, i.e.

$$0.897 \text{ mm}/(\Delta p/p) \times 10^{-4} \quad .$$

3) The beam density at the analyzing slit is assumed to be uniform across the slit width, but triangular with respect to the momentum distribution, (see Fig. 16).

Assumption (1) is justified by the fact that the beam normally used in these measurements has a divergence of only 4.5 mrad, whereas aberration tests done at $\pm$ 12 mrad showed the effects to be quite small.

The triangular distribution $J(p, x)$ along the momentum axis is essentially that due to the energy analysis performed by the first magnet. The real distribution along x is expected to be somewhat different from the simple assumption (3), and would perhaps decrease on each side of the slit center. However, it can be shown that the uniform distribution assumed here could only underestimate the beam energy resolution.

A typical example of the calculated beam profile obtained at the clean up slit position is shown in Fig. 17. From such graphs the lateral displacement

and hence the $\Delta B/B$ necessary to reduce the current transmitted through the slit to its half-value can easily be computed.

The results are shown in Fig. 18, for entrance and analyzing slit gaps of 0.5 mm and 0.75 mm, and a fixed clean-up slit of 0.5 mm.

Repeated sets of measurement gave for $\frac{2\Delta B}{B}$ values between 2 and 2.3×10^{-4}. From Fig. 18 it is deduced that the true energy resolution of the beam is

$$0.015\% \leq \left(\frac{\Delta E}{E}\right)_{FWHM} \leq 0.018\%.$$

Table 1

110° Analyzing Magnet Current Regulation

Magnet current	0-1000 A
Magnet voltage	0-110 V
DC loop gain	10^4
DC Loop band width	1 rad/sec
(corresponding to principal magnet = 1 sec)	
AC Loop gain	10^2 - 10^3
AC Loop band width	200 HZ
AC Loop crossover pole	1 rad/sec
SCR Tracking loop gain	10^2
SCR Tracking loop band width	.01 Hz
Pass transistor band width	100 kHz
Pass transistor voltage range 1000 A	4 - 20 V
Pass transistor mean voltage	12 V
Pass transistor total current rating	2 kA
Pass transistor dissipation rating	20 kW
Pass transistor h_{FE}	1×10^4
Maximum frequency for 100% modulation of current	3 Hz
Shunt	1 V 1000 A, Manganin, water cooled
DC Loop preamplifier	HP 2470A
Reference generator	1N 930A, Temperature compensated divider, manganin potentiometer

Table 2

Average Parameters Used for Shims

Region	Magnet #1		Magnet #2	
	$\bar{B}_2/\bar{B}_0$ $(in)^{-2}\times10^{-5}$	D (in)	$\bar{B}_2/\bar{B}_0$ $(in)^{-2}\times10^{-5}$	D (in)
Beam Entrance	-15 ± 2	0.45 ± 0.2	-9.7 ± 2	0.4 ± 0.2
Center Region	5 ± 1	0.16 ± 0.1	8.2 ± 0.5	0.4 ± 0.1
Beam Exit	-12 ± 2	0.15 ± 0.1	-26.0 ± 2	-0.6 ± 0.2

FIGURE CAPTIONS

Fig. 1. Beam transport system for analyzing magnets. Quartz or Al_2O_3 plates are observed with television cameras for beam focusing.

Fig. 2. Cross section of edge of magnet showing field clamp and bevelled pole edge.

Fig. 3. Plan view of 110° magnet.

Fig. 4. Beam envelope from entrance slit to analyzing slit.

Fig. 5. Calculated aberration at analyzing slit for uniform field magnet.

Fig. 6. Calculated aberration at analyzing slit for ideally shimmed field.

Fig. 7. Method of estimating the effect of aberrations on the momentum resolution.

Fig. 8. Cross section of iron, coil and vacuum tank.

Fig. 9. Block diagram of current regulator.

Fig. 10. Azimuthal variation of field at magnet edge, measured at three different radii for 2092 gauss field.

Fig. 11. Azimuthal variation of field in central region of magnet, measured at various radii for 5225 gauss field. Position of zero variation is arbitrary. For clarity curves are arbitrarly displaced relative to one another.

Fig. 12. Radial variation of azimuthally averaged field for central region of magnet II.

Fig. 13. Radial variation of field at end of magnet.

Fig. 14. Definition of quantities for shim calculations.

Fig. 15. $^{12}C(p, p)^{12}C$ resonance at 14.233 MeV (lab).

Fig. 16. Assumed beam intensity J(p, x) at exit of analyzing slit as a function of radial position x and momentum p.

Fig. 17. Calculated beam intensity $J(x)$ at clean-up slit, assuming beam distribution shown in Fig. 16.

Fig. 18. Finite slit-width corrections to be applied to measured $\Delta E/E$.

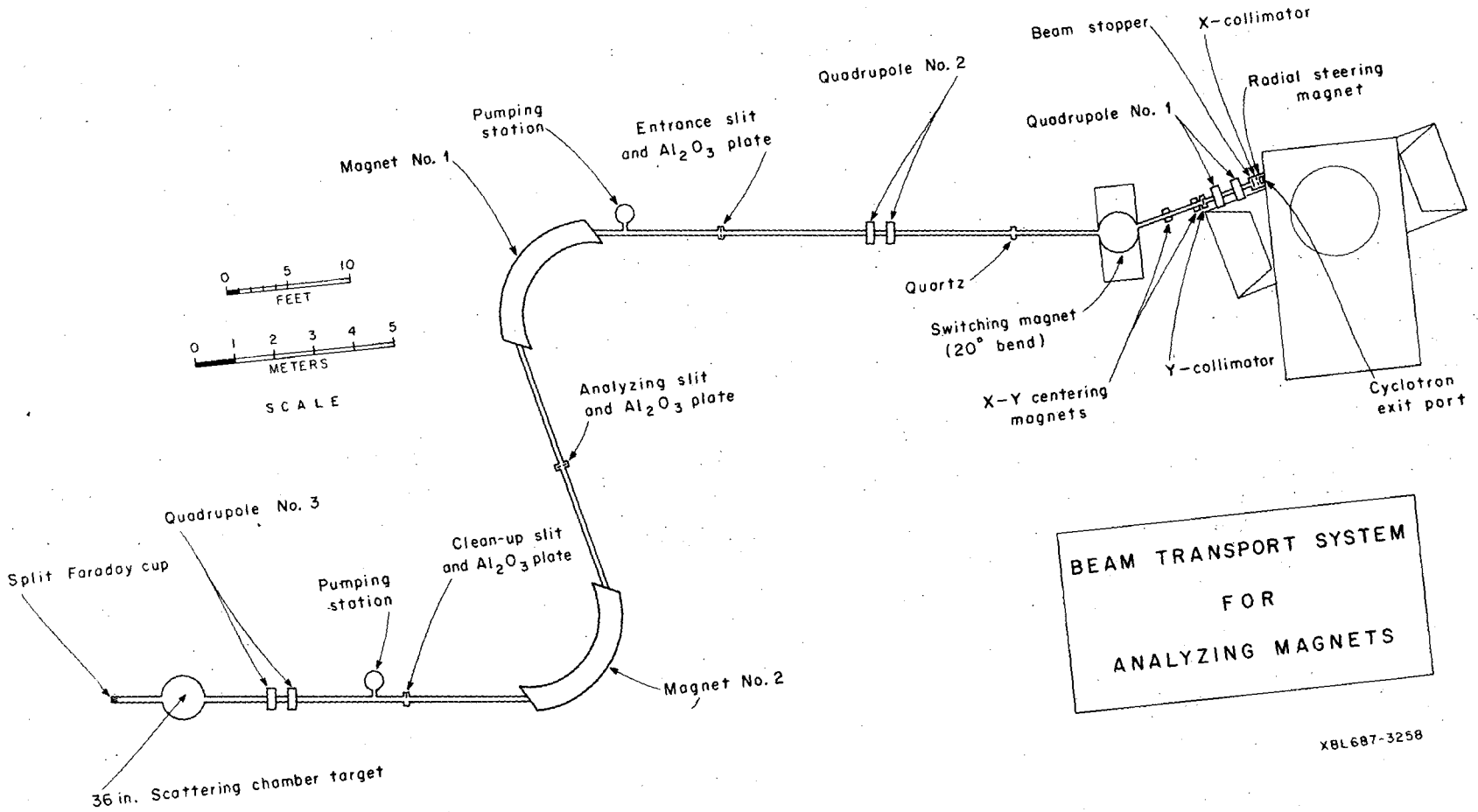

BEAM TRANSPORT SYSTEM
FOR
ANALYZING MAGNETS

XBL687-3258

Fig. 1.

UCRL-18383

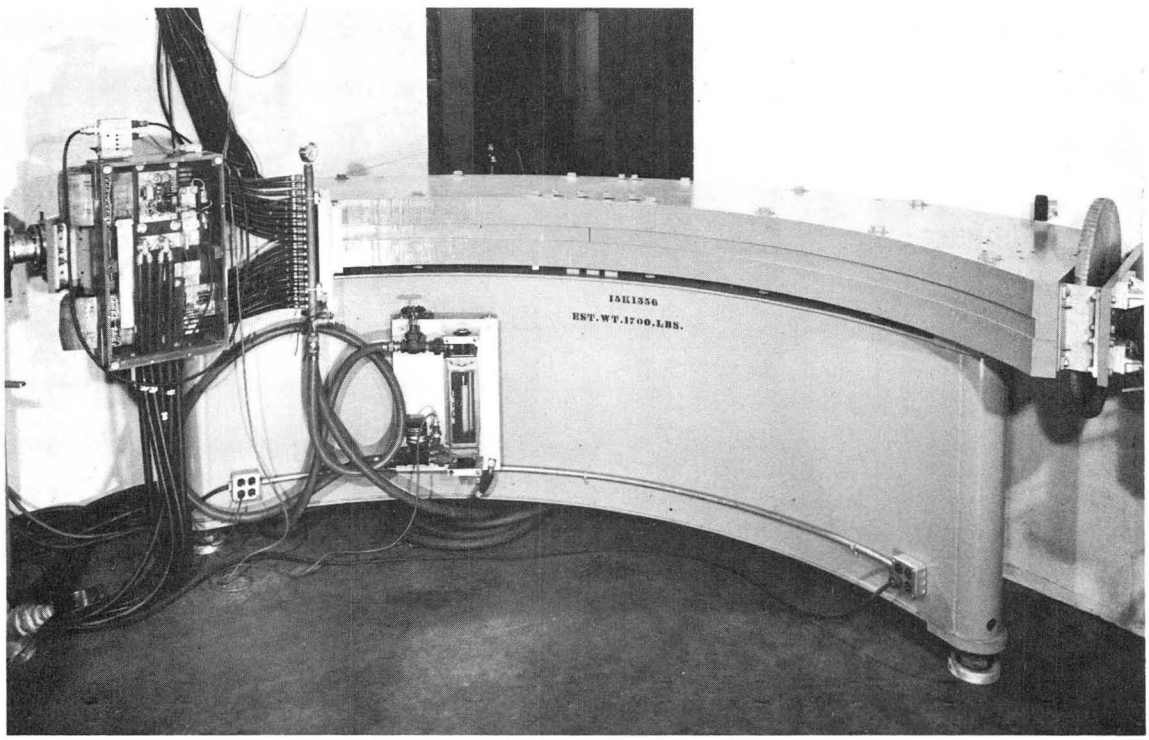

XBB 688-4699

Fig. 1a

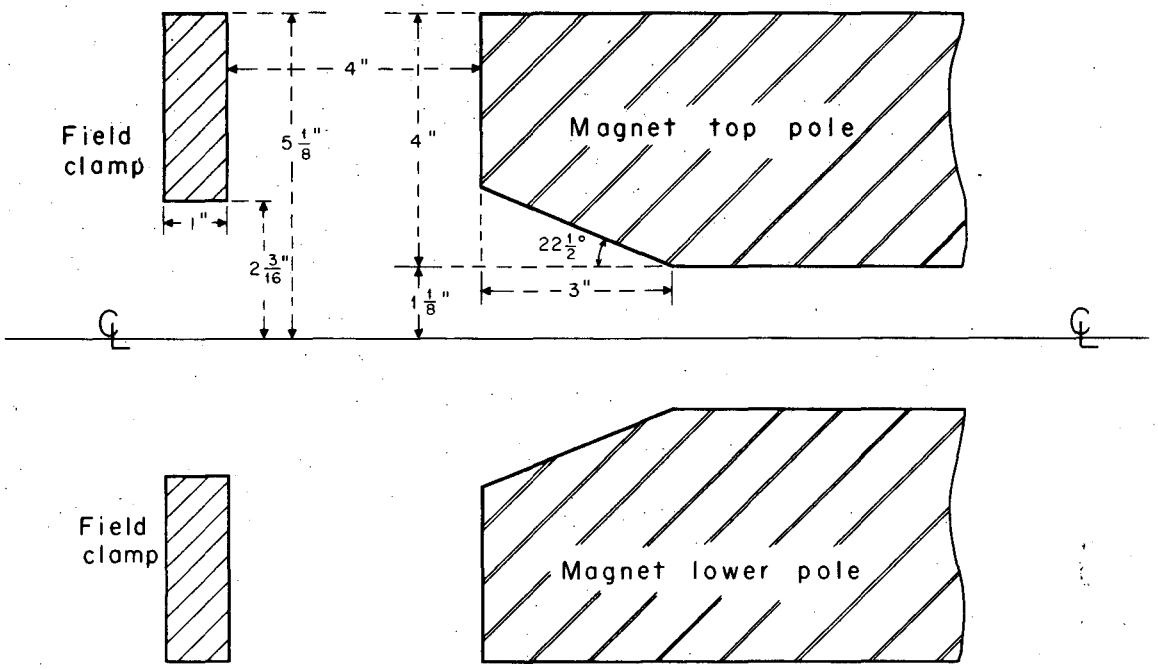
Field clamp
4"
5 1/8"
4"
Magnet top pole
1"
2 3/16"
22 1/2°
3"
1 1/8"
Field clamp
Magnet lower pole
XBL687-3271

Fig. 2.

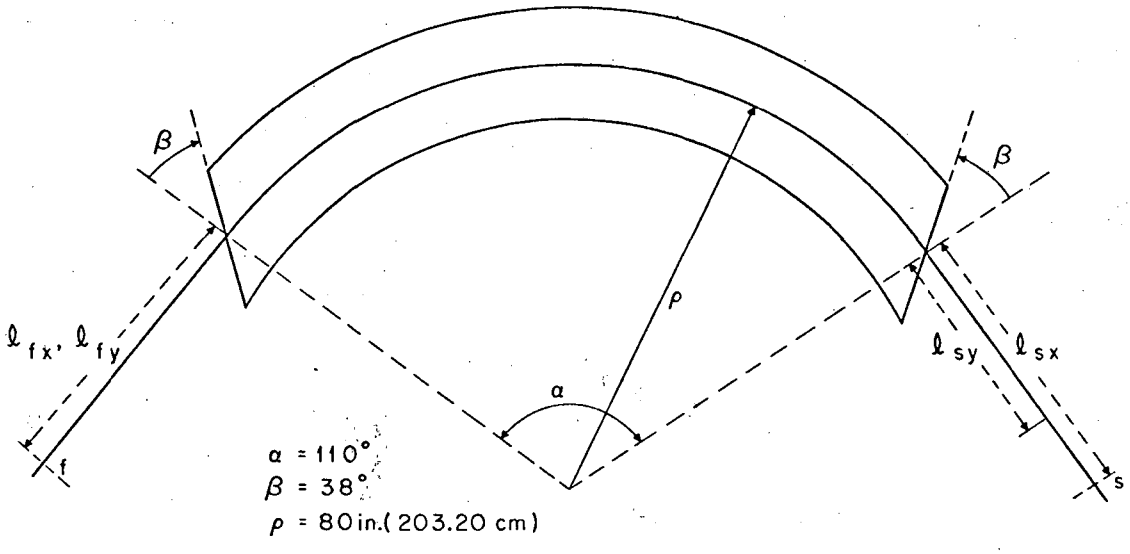
β
β
ρ
α
ℓ_{fx}, ℓ_{fy}
ℓ_{sy}
ℓ_{sx}
f
s
α = 110°
β = 38°
ρ = 80 in. (203.20 cm)
XBL687-3270

Fig. 3.

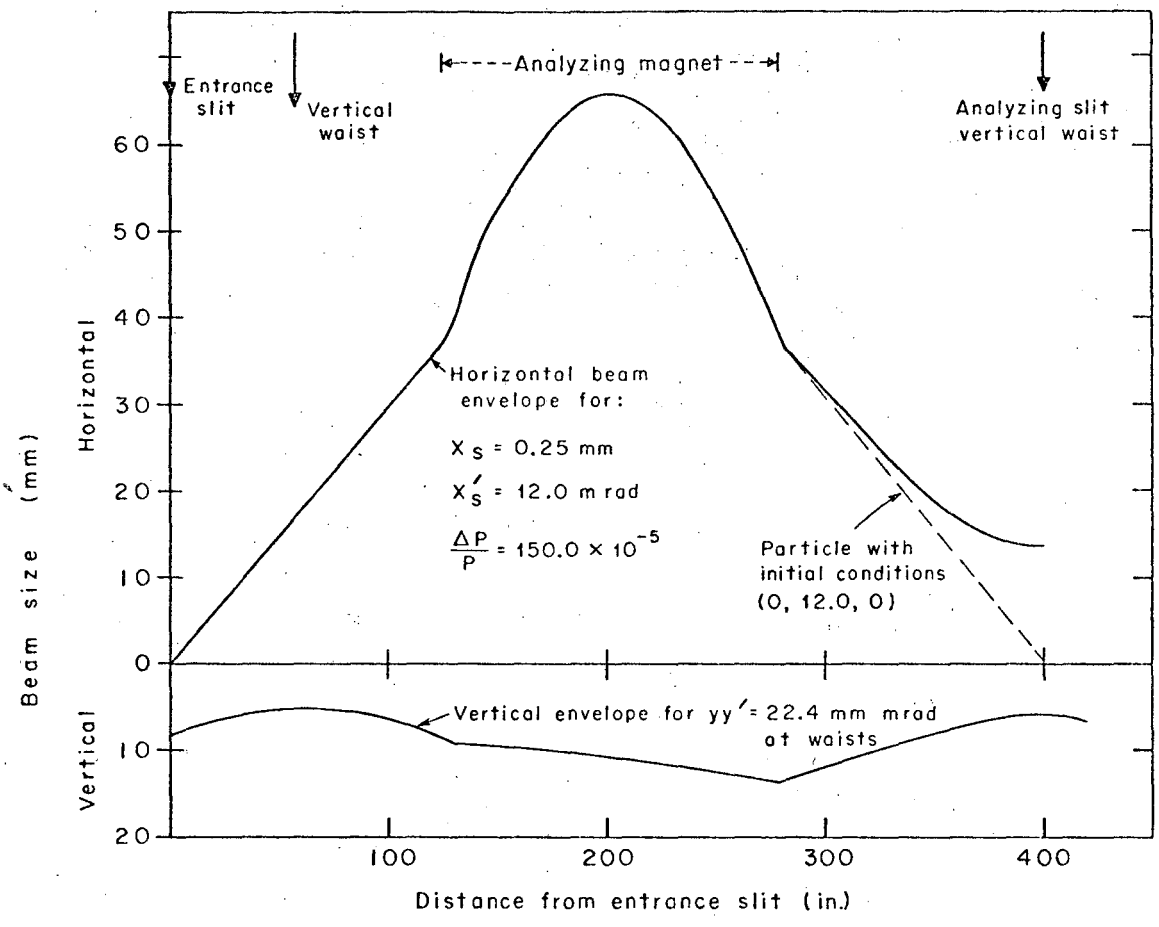

XBL687-3269

Fig. 4.

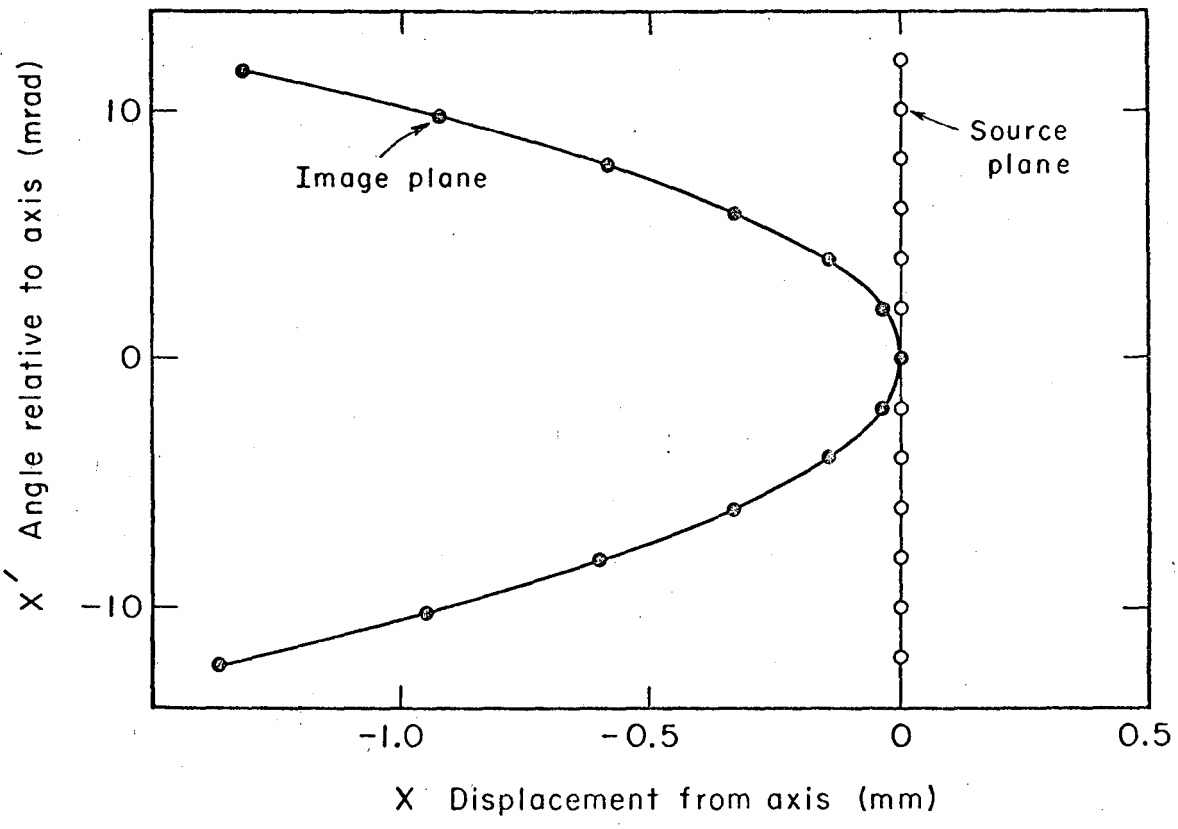

XBL687-3265

Fig. 5.

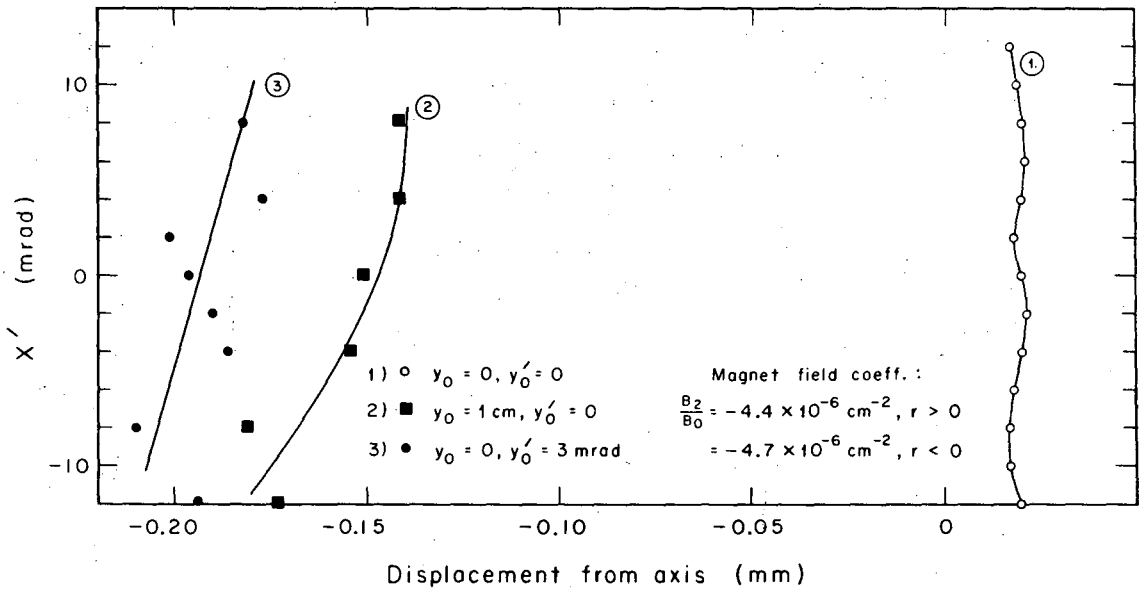

XBL687-3267

Fig. 6.

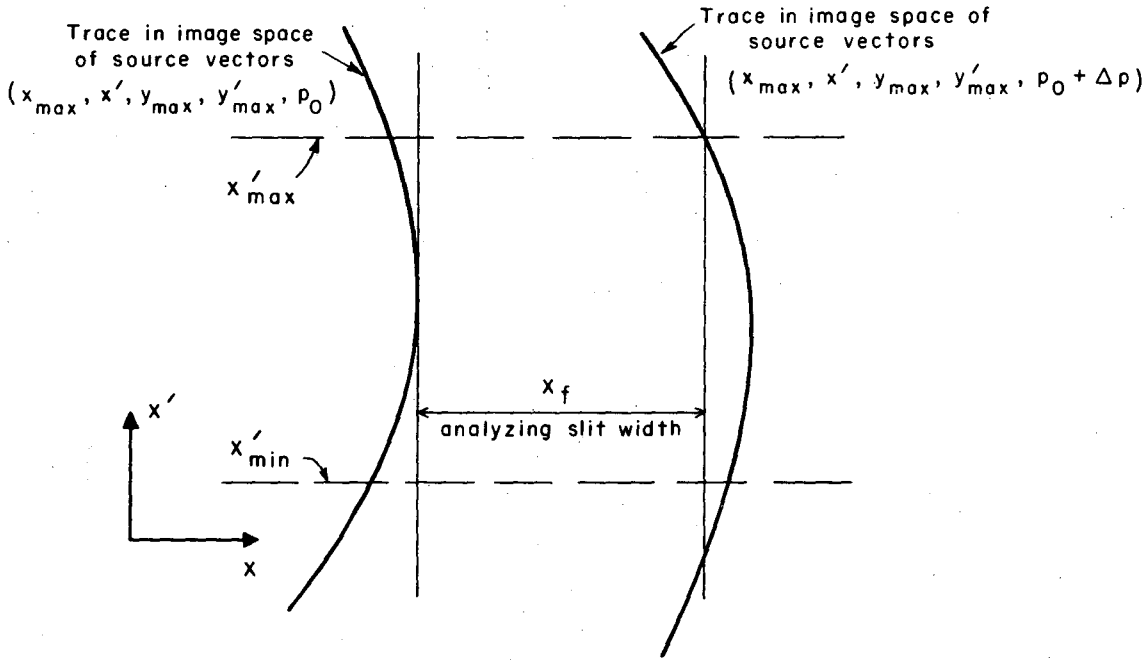

XBL687-3452

Fig. 7.

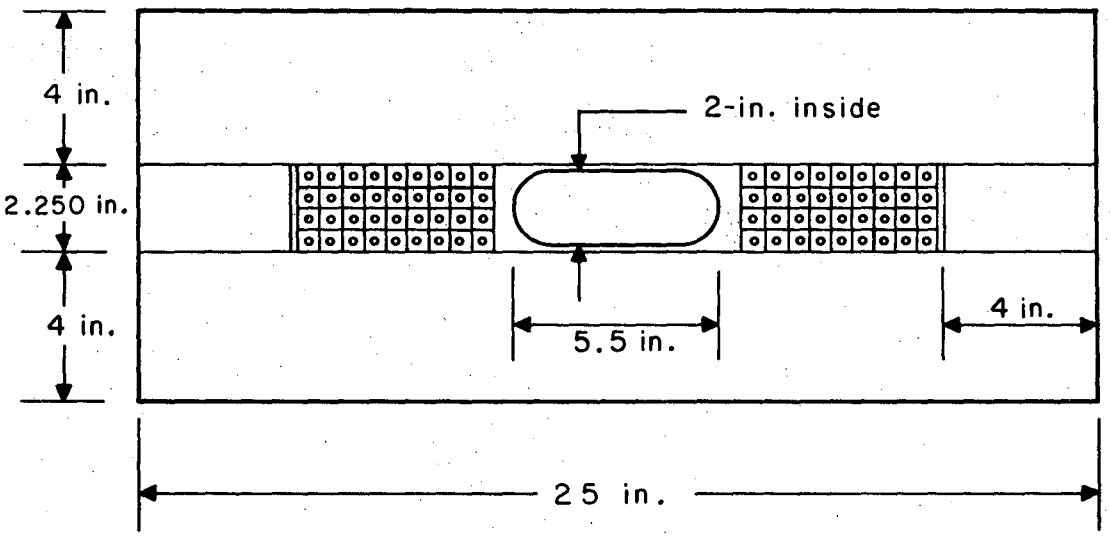

XBL687-3266

Fig. 8.

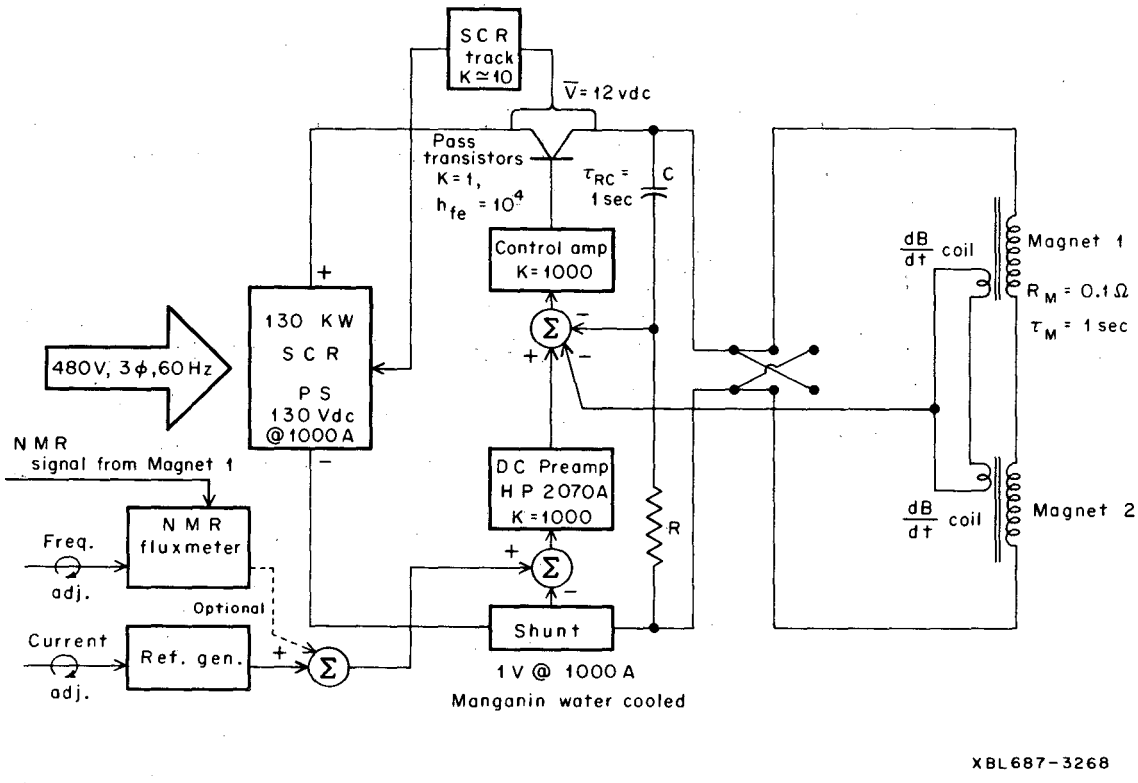

XBL687-3268

Fig. 9.

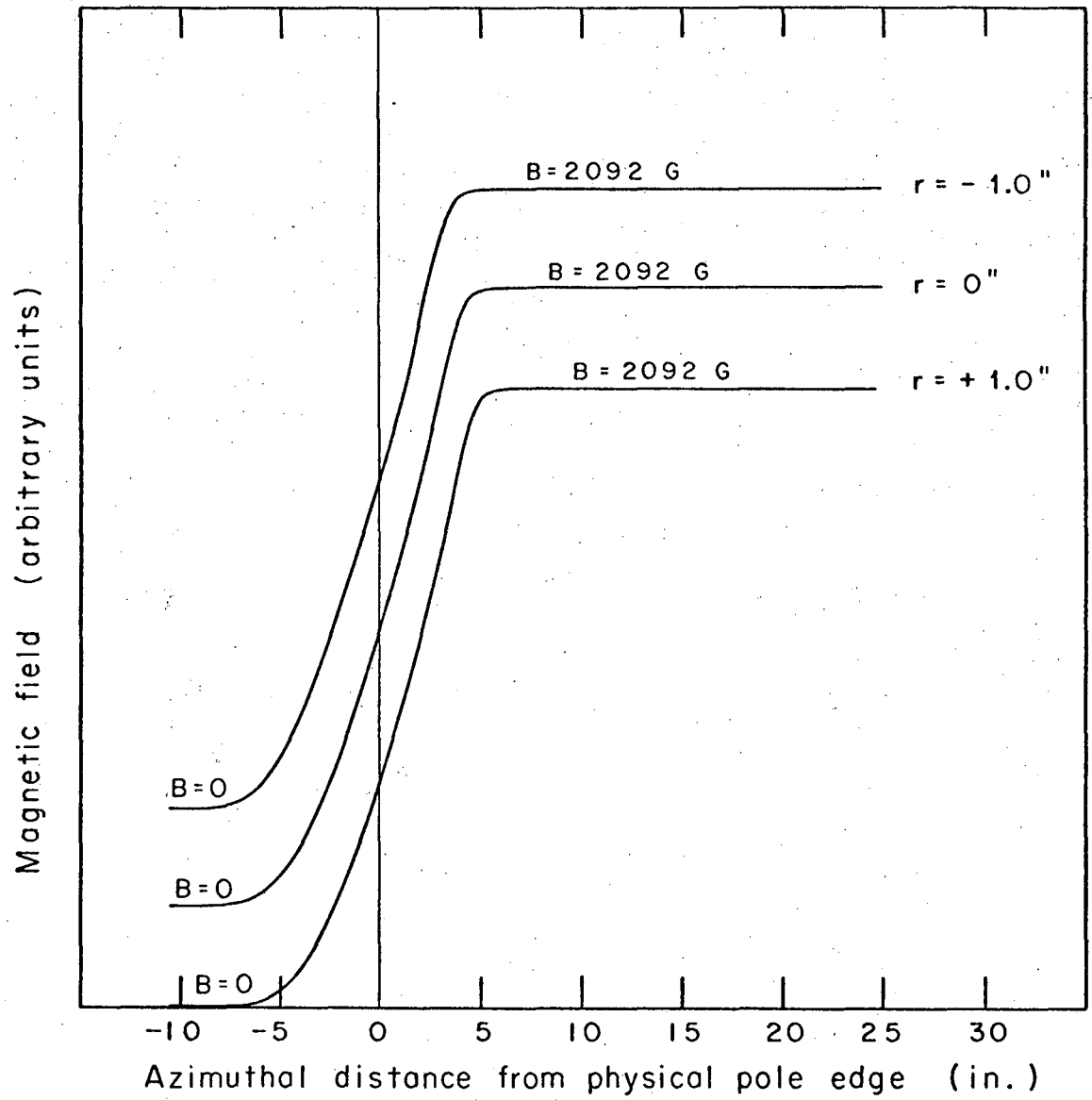

XBL687-3262

Fig. 10.

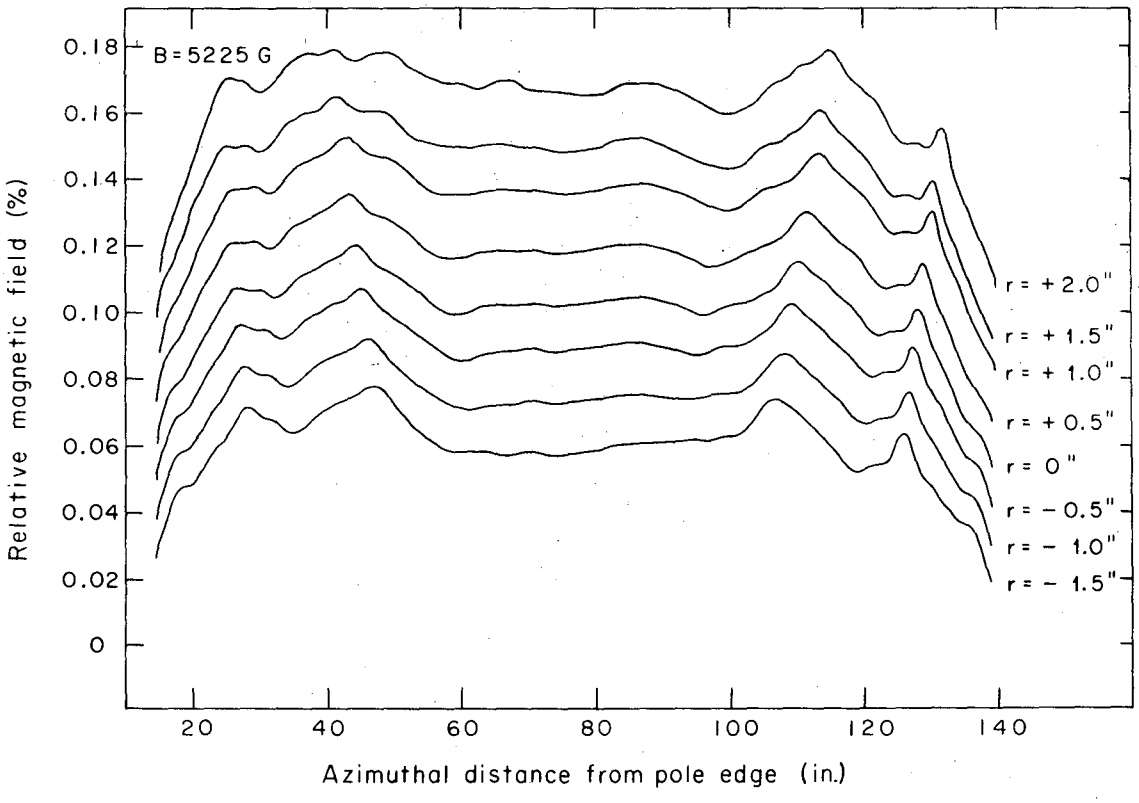
B = 5225 G
Relative magnetic field (%)
0.18
0.16
0.14
0.12
0.10
0.08
0.06
0.04
0.02
0
20
40
60
80
100
120
140
Azimuthal distance from pole edge (in.)
r = + 2.0"
r = + 1.5"
r = + 1.0"
r = + 0.5"
r = 0"
r = − 0.5"
r = − 1.0"
r = − 1.5"
XBL687-3263

Fig. 11.

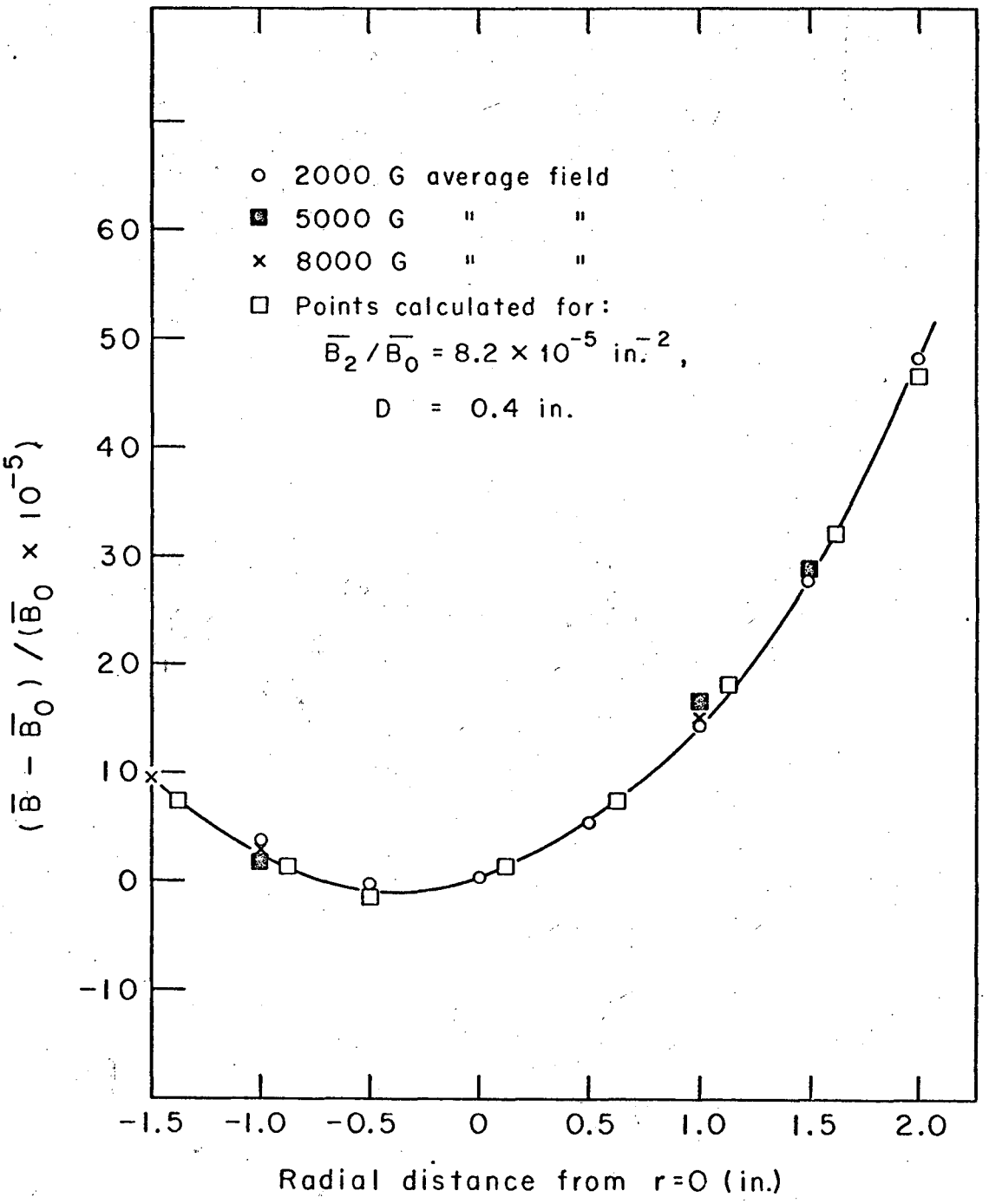

XBL 687-3353

Fig. 12.

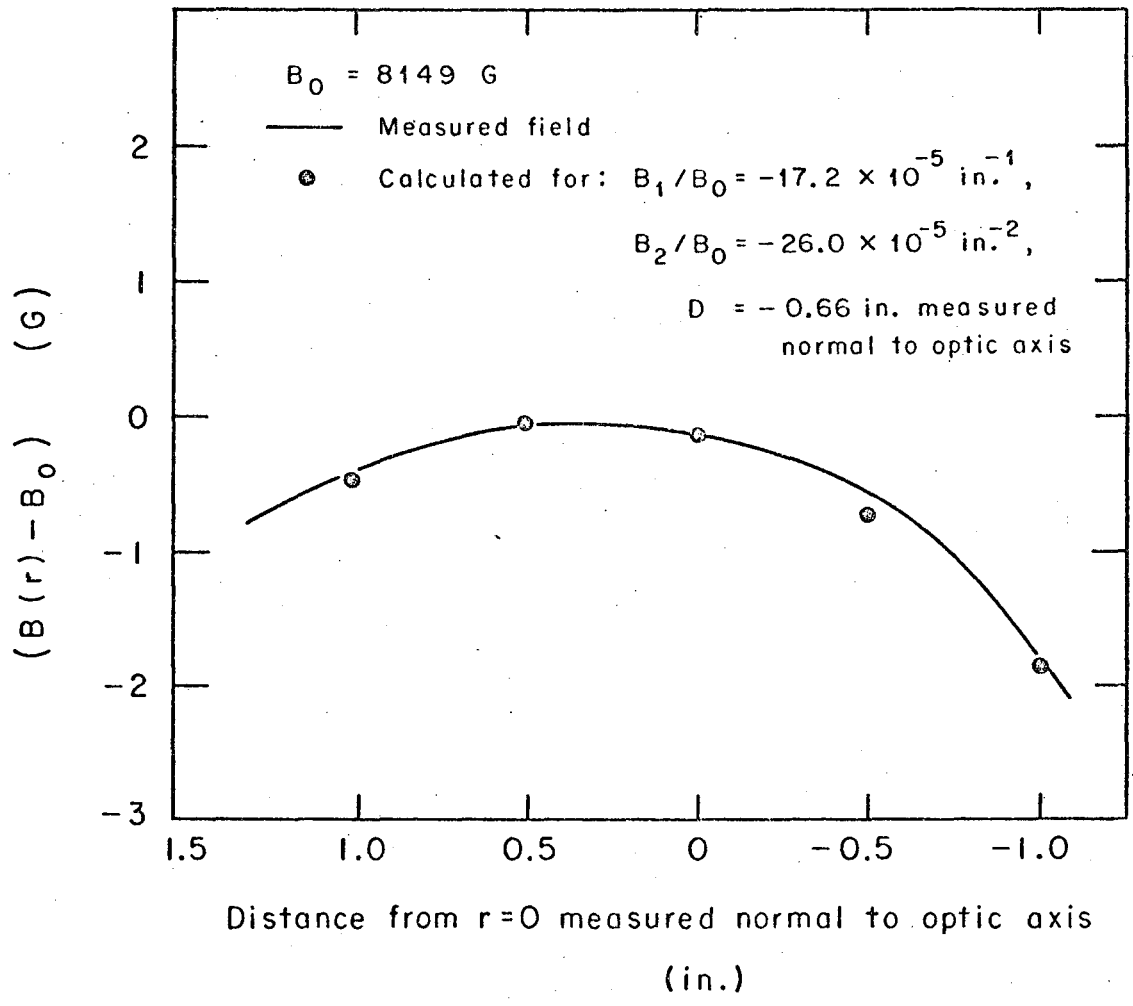

XBL687-3264

Fig. 13.

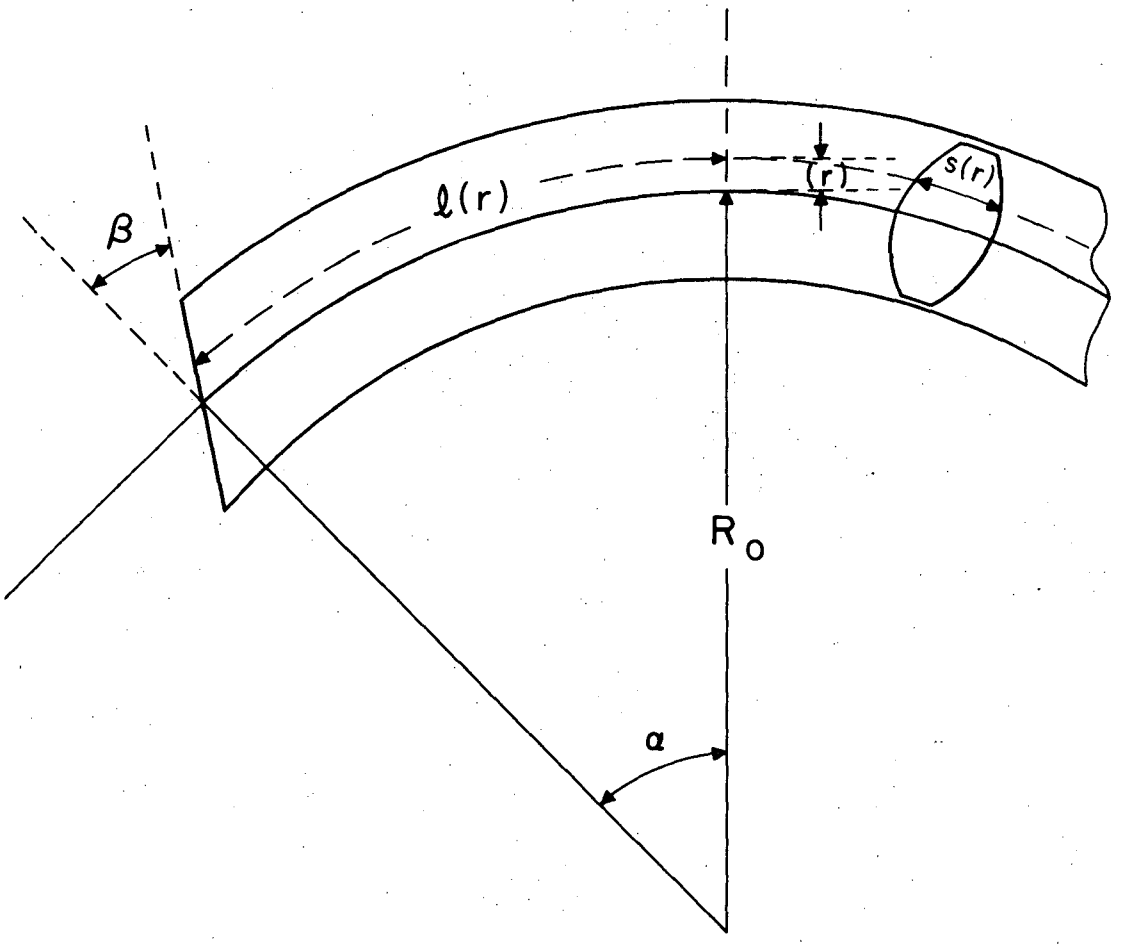

XBL687-3261

Fig. 14.

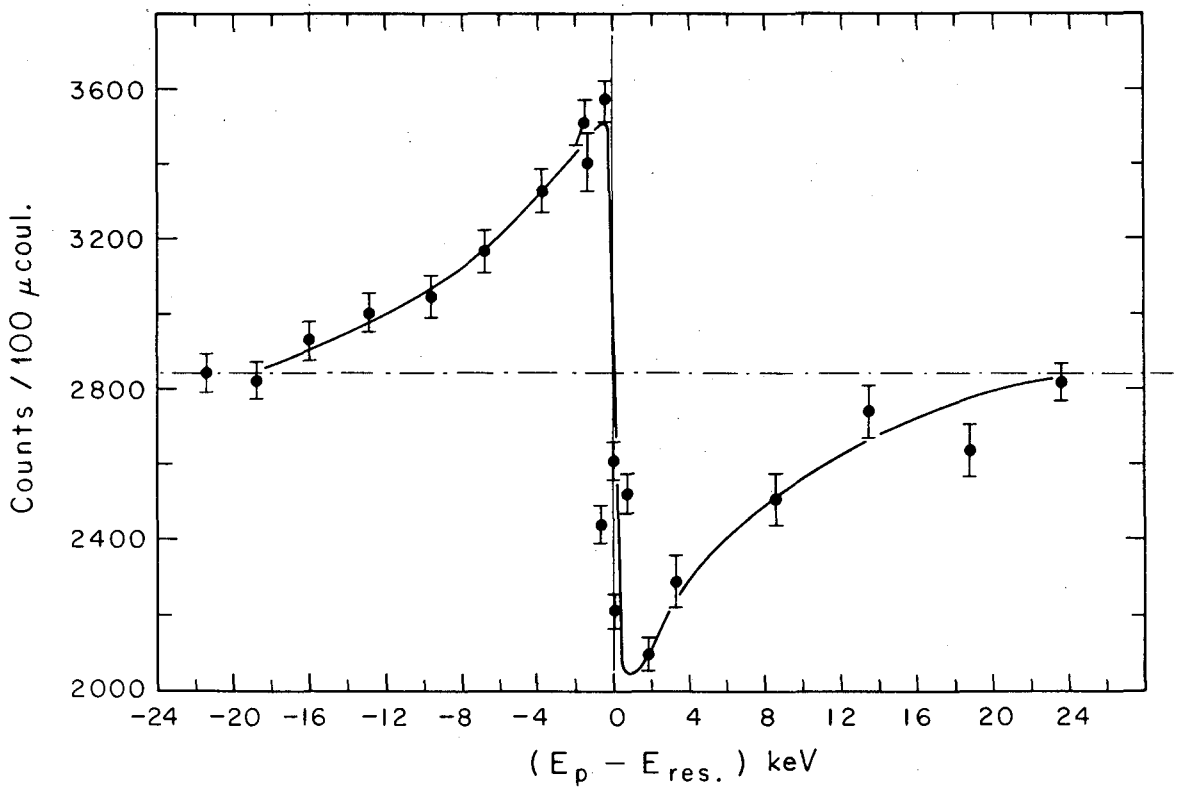
Counts / 100 μcoul.
3600
3200
2800
2400
2000
-24
-20
-16
-12
-8
-4
0
4
8
12
16
20
24
(E_p − E_res.) keV
XBL687-3260

Fig. 15.

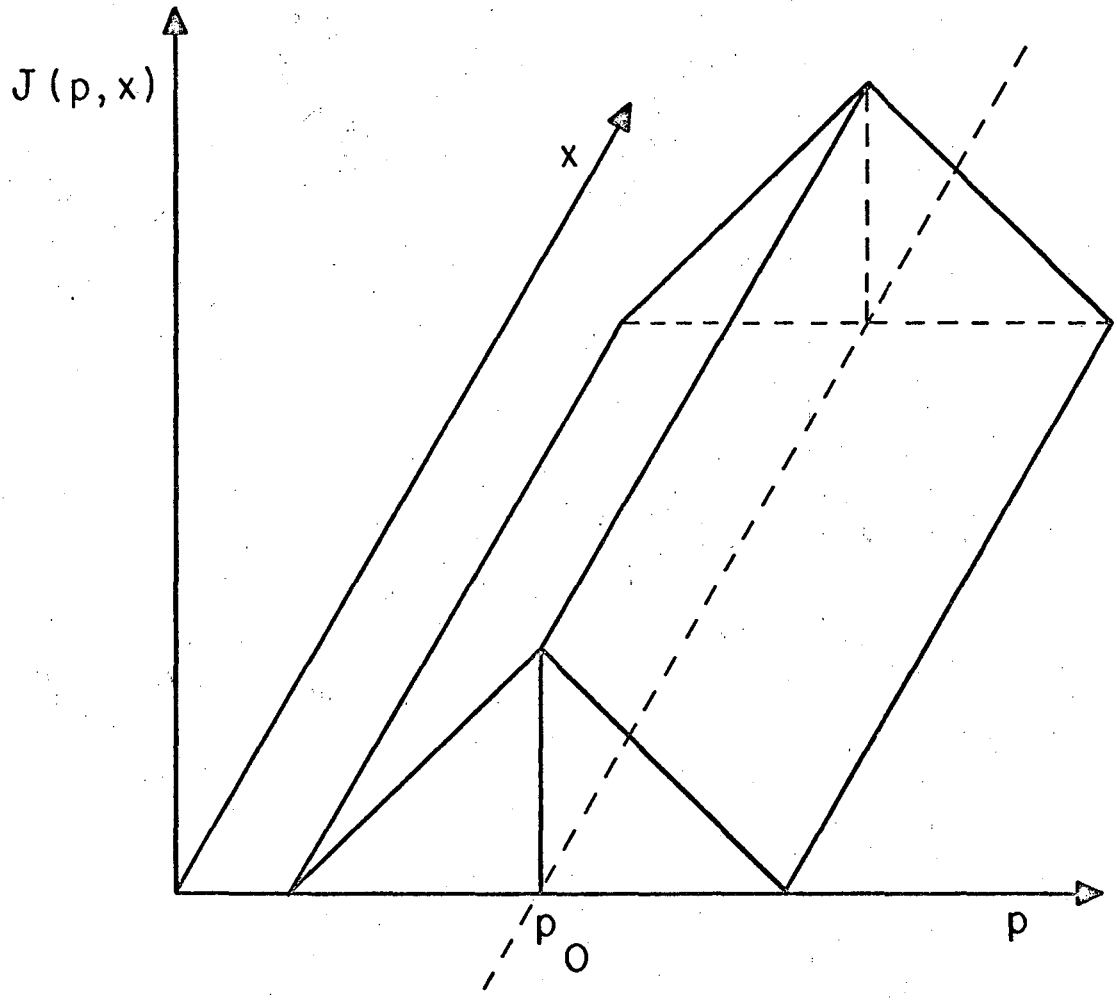

XBL688-3539

Fig. 16.

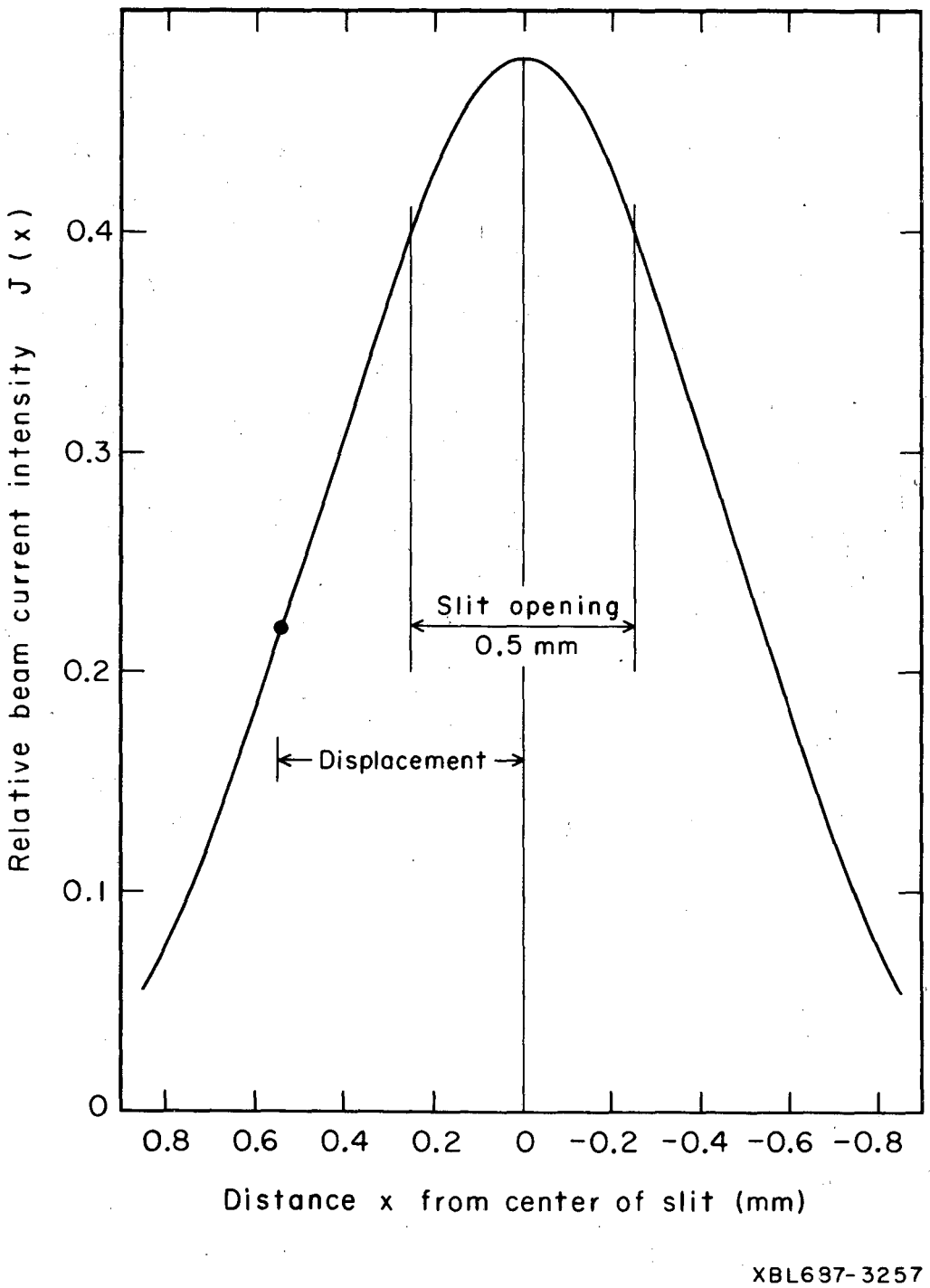
Relative beam current intensity J(x)
0.4
0.3
0.2
0.1
0
Slit opening
0.5 mm
Displacement
0.8 0.6 0.4 0.2 0 -0.2 -0.4 -0.6 -0.8
Distance x from center of slit (mm)
XBL697-3257

Fig. 17.

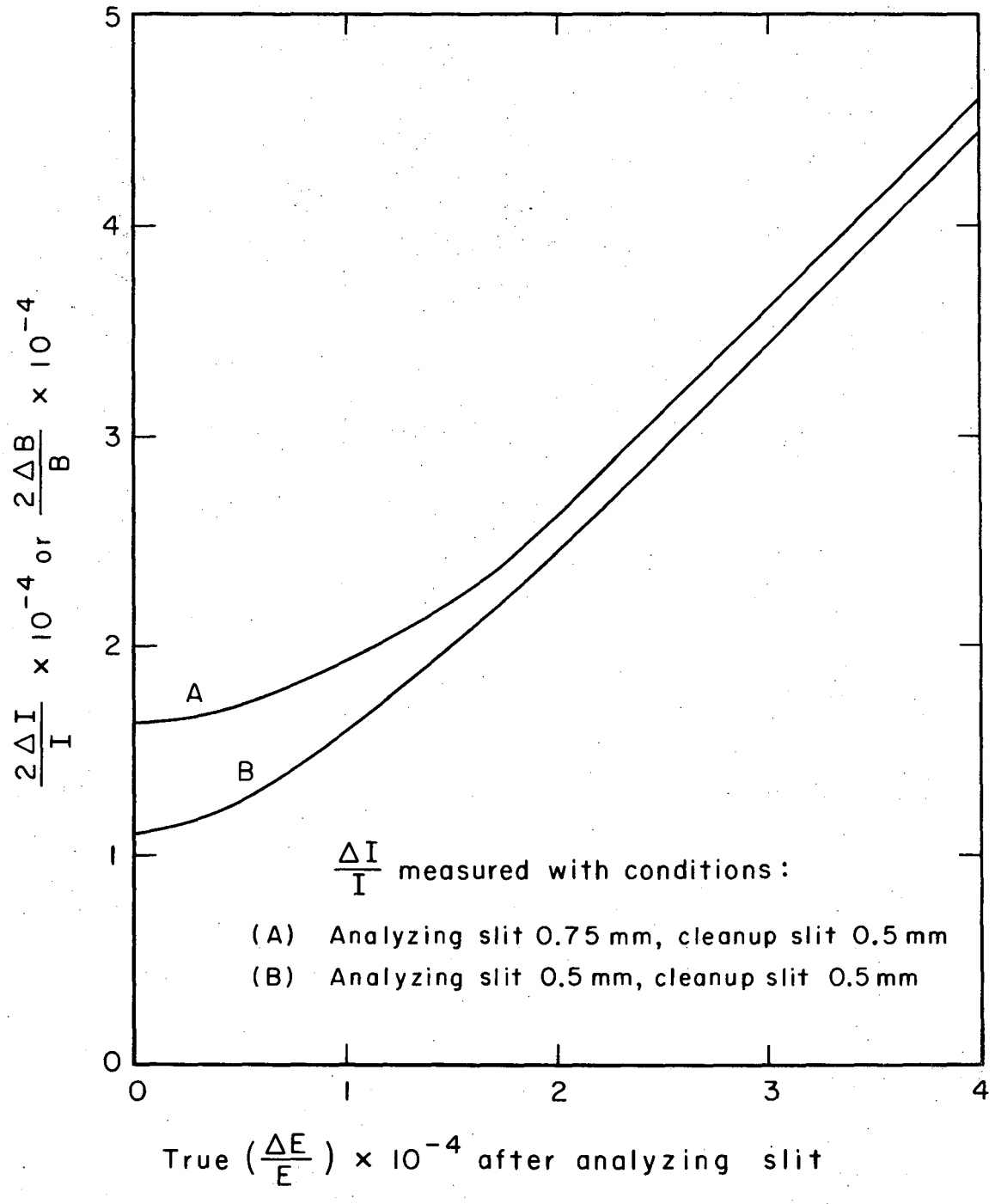

XBL687-3259

Fig. 18.

LEGAL NOTICE

TECHNICAL INFORMATION DIVISION
LAWRENCE RADIATION LABORATORY
UNIVERSITY OF CALIFORNIA
BERKELEY, CALIFORNIA 94720